TR－A－0144

Virtual Trajectory and Stiffness Ellipse During Multi-Joint Arm Movement Predicted by Neural Inverse Models

Masazumi KATAYAMA　Mitsuo KAWATO

1992. 4. 30

ATR視聴覚機構研究所

〒619-02 京都府相楽郡精華町光台2-2 ☎07749-5-1411

ATR Auditory and Visual Perception Research Laboratories

2-2, Hikaridai, Seika-cho, Soraku-gun, Kyoto 619-02 Japan

Telephone: +81-7749-5-1411
Facsimile: +81-7749-5-1408

Virtual Trajectory and Stiffness Ellipse During Multi-Joint Arm Movement Predicted by Neural Inverse Models

Masazumi KATAYAMA[1*] and Mitsuo KAWATO[2]

[1] Cognitive Processes Department
ATR Auditory and Visual Perception Research Laboratories
Hikaridai, Seika-cho, Soraku-gun, Kyoto 619-02, Japan

[2] Department III
ATR Human Information Processing Research Laboratories
Hikaridai, Seika-cho, Soraku-gun, Kyoto 619-02, Japan
E-mail kawato@atr-hr.atr.co.jp

* present address: Sanyo Electric Co., Ltd., Tsukuba Research Center, Intelligent Systems Laboratory, 2-1 Koyadai, Tsukuba Ibaraki 305 Japan
E-mail katayama%tsukuba.sanyo.co.jp@uunet.uu.net

All correspondences should be addressed to Mitsuo Kawato
Tel: 81-7749-5-1040, Fax: 81-77495-1008

Abstract

Because of the long delays associated with neural feedback loops, feedforward control is essential for relatively fast movements. Two approaches explaining the feedforward control of voluntary movements have been proposed in computational neuroscience for motor control. One avoids explicitly computing the inverse dynamics problem, and the other solves the problem by using learned internal models of the motor systems. In the former approach, a *virtual trajectory control* hypothesis has been intensively studied. According to this hypothesis, the brain computes the virtual trajectory and does not need to worry about low-level control problems. If experimentally observed roughly straight hand trajectories can be produced from such simple virtual trajectories as the straight minimum-jerk trajectory, complicated computations associated with the inverse dynamics problem need not be addressed. Thus, trajectory planning and control can be very simply performed. This paper compares the computational complexity of planning the virtual trajectory with that of solving the inverse dynamics problem. Computer simulations are performed using stiffness values during movement measured by Bennett et al. (Bennett, 1991; Bennett, Hollerbach, Xu, Hunter, 1992). The virtual trajectories and stiffness ellipses are predicted by neural network models which solve the inverse dynamics problem. The shape and orientation of the stiffness ellipses predicted during posture maintenance are similar to those measured in human experiments. The stiffness ellipses during movements depended greatly on the orientation, amplitude, and speed of movements. The virtual trajectories were much more complex than the actual trajectories. This indicates that planning the virtual trajectory is as difficult as solving the inverse dynamics problem, at least for fast movements. Finally, we propose a computational framework to integrate the virtual trajectory control hypothesis and learning neural internal models.

1 Introduction

Voluntary arm movements should be explained by feedforward and feedback control mechanisms. Control mechanisms using only feedback cannot explain how deafferented monkeys can move their arms to a target without concurrent visual information (Polit, Bizzi, 1979). The final position control hypothesis that takes account of only the final target point (Bizzi, Polit, Morasso, 1976), cannot explain how an intact monkey arm perturbed while moving toward a target returned to an intermediate point on the planned trajectory (Bizzi, Accornero, Chapple, Hogan, 1984). Moreover, feedback control is limited by the delays associated with neural feedback loops: about 100 msec for feedback through a transcortical loop, and at least 150 msec for visual feedback. In systems with long delays, only slow movements can be executed stably by feedback control, because a large feedback gain gives rise to instability. Feedforward control therefore appear to be essential for fast movements. The fundamental question here is how the central nervous system (CNS) executes feedforward control. Two approaches for feedforward motor control have been proposed. One approach is that viscoelastic properties of musculoskeletal system are utilized to avoid intensive computations required for solving the inverse dynamics problem. The other approach resolves the inverse dynamics and kinematics problems based on learned internal models of motor systems (see, for example, Kawato, Furukawa, Suzuki, 1987; Katayama and Kawato, 1991a; Gomi and Kawato, 1990).

Our objective in this paper is to systematically compare the computational difficulties of the two approaches. Let us first review briefly the former approach. The visco-elastic properties of the neural-musculoskeletal system play an important role in controlling posture and movement. Rack and Westbury (1974) examined the length-tension curve of an individual muscle under isometric conditions and quantitatively ascertained that muscles exhibit spring-like behavior. This muscle elasticity depends on the activation level of the muscle itself, and a higher muscle activation level results in greater stiffness. Fel'dman (1966,1990) studied how the CNS makes use of such elastic muscle behavior and proposed that posture is determined by the equilibrium point of the length-tension curves of agonist and antagonist muscles, well known as the equilibrium point hypothesis.

Hogan (1984) proposed the virtual trajectory control hypothesis. A virtual trajectory was defined as a series of equilibrium points generated by gradually shifting the equilibrium posture.

Virtual trajectory control for multi-joint arm movements is described by the following equation.

$$M(\theta)\ddot{\theta} + C(\theta,\dot{\theta})\dot{\theta} + G(\theta) = \tau, \qquad (1a)$$

$$\tau = J^T S(x_v - x), \qquad (1b)$$

$$\dot{\theta} = \frac{d\theta}{dt}, \quad \ddot{\theta} = \frac{d^2\theta}{dt^2}, \quad x = L(\theta), \quad J = \frac{\partial X}{\partial \theta}.$$

Here x and θ are the actual hand position and joint angle vectors; $M(\theta)$ is the inertia matrix; $C(\theta,\dot{\theta})$ is the matrix that expresses the centrifugal, Coriolis and friction forces; $G(\theta)$ is the vector of the joint torque due to gravity; τ is the torque vector around the joint; $L(\theta)$ is the forward kinematics equation; and J is its Jacobian matrix. In this framework, the joint torque τ required for an intended trajectory are automatically generated by multiplying the difference between the virtual trajectory x_v and the actual trajectory x by the hand stiffness S. The actual trajectory is therefore determined by the interaction of this elastic force with the dynamic forces caused by the terms M, C and G. Thus, the inverse dynamics problem is solved implicitly, since the joint torque is generated without any explicit torque computation. In this control hypothesis, the main role of the brain is to send the virtual trajectory and a series of stiffnesses to the periphery, without considering low-level control problems. The advantages of this hypothesis are that the viscoelastic properties of the musculoskeletal system are efficiently utilized, the inverse dynamics problem is avoided, and force control as well as trajectory control can be dealt with. Such control schemes, however, do not readily explain biological motor learning.

If the hand stiffness S during movement is much greater than the at-rest stiffness during posture maintenance, the virtual trajectory x_v is similar to the actual trajectory x. On the other hand, if S is not large enough, the virtual trajectory differs significantly from the actual trajectory. The profile of such a virtual trajectory therefore strongly depends on the value of S during movement. The CNS must either increase the stiffness or modify the virtual trajectory, because the dynamic forces for fast movements become large. For example, inertia and interaction force increase is proportional to the square of the inverse of movement time. Hogan (1984) simulated a single-joint movement, and found that in faster movements the virtual trajectory was initially overshot but that this overshoot could be eliminated by increasing the stiffness while keeping the same damping ratio. To quantitatively assess the computational difficulty of the virtual trajectory control hypothesis, it is therefore necessary to measure stiffness values during movements. Mussa-Ivaldi, Hogan and Bizzi (1985) measured and characterized the field of elastic forces associated with hand posture in the horizontal plane. The measured stiffness ellipses were approximately oriented with the major axis pointing towards the shoulder, and the shape and orientation of the ellipses of a fixed posture were somewhat invariant for different subjects and different days, with only their size changing.

The human hand trajectories for point-to-point movements are roughly straight, with a bell-shaped tangential velocity profile (horizontal plane: Morasso, 1981; Abend, Bizzi, Morasso, 1982; Flash and Hogan, 1985; Uno, Kawato, Suzuki, 1989a. vertical plane: Atkeson and Hollerbach, 1985). This indicates that the virtual trajectories must be planned by taking into account spatial anisotropies in the stiffness ellipses, while the actual trajectories are roughly straight isotropically. Flash (1987) simulated multi-joint arm movements based on virtual trajectory control, and concluded that the actual human arm trajectories could be reproduced by assuming straight virtual trajectories. Planning the straight virtual trajectories is obviously easier than directly solving the inverse dynamics problem. Flash (1987), however, assumed that the coefficients of the joint stiffness matrix during movements of one-second duration are two to three times larger than the values measured by Mussa-Ivaldi et al. (1985), and manually adjusted the coefficients so as to reproduce the actual arm movements. When 500-msec movements are executed based on this assumption, the coefficients must be about 10 times as large as their static values during posture maintenance, because the dynamic forces during half-duration increase roughly four times.

2. Learning of neural inverse models

Insert Figure 1 around here

Kawato et al. (1987) expanded conceptual models that show that the voluntary movements are accomplished using internal models of the motor systems (Ito, 1970; Tsukahara and Kawato, 1982), and proposed a *hierarchical neural network* model for controlling and learning voluntary movements. This model uses a *feedback-error-learning* scheme, which is a supervised-motor-learning scheme, to acquire the inverse kinematics model and/or the inverse dynamics models of the controlled object. By further developing this neural network model, Katayama and Kawato (1991a) proposed a *parallel-hierarchical neural network* model, that uses also the feedback-error-learning scheme, to acquire inverse statics and dynamics models.

We briefly review our parallel-hierarchical neural network model. The dynamics equation of a multi-joint arm can be written as

$$M(\theta)\ddot{\theta}+C(\theta,\dot{\theta})\dot{\theta}+G(\theta)=\tau(\theta,\dot{\theta},u), \qquad \text{(2a)}$$

$$\tau(\theta,\dot{\theta},u)=A(\theta)^T T(l,\dot{l},u), \qquad \text{(2b)}$$

$$\dot{l}=\frac{dl}{dt}.$$

Here $\tau(\theta,\dot{\theta},u)$ is the joint torque generated by agonist and antagonist muscles and the other notations are similar to (1a). The vector variable u is the motor command fed to the muscles, and θ is the joint angle. $T(l,\dot{l},u)$ is the muscle tension vector and l is the muscle length vector. The dimension of vectors, θ and τ, are equal to the number of joints n. The dimension of vectors, u, T, and l, are equal to the number of muscles m, and m is greater than n. The matrix $A(\theta)$ is the $n\times m$ moment arm matrix and depends on the joint angle θ.

If the arm is static ($\dot{\theta}=\ddot{\theta}=\dot{l}=0$), then Equations (2a) and (2b) are reduced to

$$A(\theta)^T T(l,0,u)-G(\theta)=0. \qquad \text{(3)}$$

This is a statics equation. The problem of calculating the motor commands from a desired joint angle vector using this equation is defined as the *inverse statics* problem. There are two difficulties: first, Equation (3) includes the nonlinear functions $A(\theta)$, $T(l,0,u)$, and $G(\theta)$. We need, therefore, to solve these nonlinear equations. Second, as discussed below, the inverse statics is an ill-posed problem. These difficulties, however, can be solved by training the inverse statics model ISM. The problem of computing dynamic torque other than that calculated from (3) is called the *inverse dynamics* problem and is solved by training the inverse dynamics model IDM. The main role of the ISM is to control the equilibrium posture and mechanical stiffness, and that of the IDM is to compensate for the dynamic properties of the arm during fast movements. The ISM control is closely related to the virtual trajectory control. The parallel-hierarchical neural network model arranges these parallel inverse models hierarchically in conjunction with a feedback controller (Fig. 1). The motor command for agonist and antagonist muscles is the sum of the three outputs, u_{ism}, u_{idm}, and u_{fc}, which are calculated by the ISM, the IDM, and the feedback controller. In this study, the ISM and IDM are structured as multi-layer neural network models with synaptic weights w. These two inverse models can be described as mappings from the desired trajectory θ_d to motor command u:

$$u_{ism} = \Psi_{ism}(w_{ism}, \theta_d), \tag{4a}$$

$$u_{idm} = \Psi_{idm}(w_{idm}, \theta_d, \dot{\theta}_d, \ddot{\theta}_d). \tag{4b}$$

To obtain the parallel inverse models, the synaptic weights of the ISM and IDM are modulated by a combination of the following feedback-error-learning algorithm (Kawato et al., 1987) and the back-propagation algorithm for hidden units (Rumelhart, Hinton, Williams, 1986).

$$\frac{dw_{ism}}{dt} = \left(\frac{\partial \Psi_{ism}}{\partial w_{ism}}\right)^T u_{fc}, \tag{5a}$$

$$\frac{dw_{idm}}{dt} = \left(\frac{\partial \Psi_{idm}}{\partial w_{idm}}\right)^T u_{fc}. \tag{5b}$$

The ISM learns while the arm is static and the IDM learns while it is moving. Before learning, the arm is controlled mainly by the feedback controller but after learning, because the feedback signal is minimized by the learning procedure, feedforward control is performed mainly by the parallel inverse models.

The ISM has three advantages: it can simultaneously control both the posture and the force (Katayama and Kawato, 1991b). Second, ISM control explains the results of Bizzi's experiment with intact and deafferented rhesus monkeys (Bizzi et al., 1984). Third, it is easy to learn the inverse dynamics model because it is separated into the ISM and the IDM.

Insert Figure 2 around here

The human arm is redundant at the dynamics level because the joint torque is generated by both agonist and antagonist muscles (Fig. 2). Acquisition of the inverse model is therefore an ill-posed problem in the sense that the muscle tensions cannot be determined uniquely from the prescribed trajectory and force. The CNS can solve such ill-posed problems by applying suitable constraints. We believe that smoothness is the fundamental principle of coordinated movements. Uno, Suzuki and Kawato (1989b) proposed a *minimum-muscle-tension-change* model that closely reproduces human arm movements. This model generates the optimum trajectory by minimizing an objective function,

$$C_T = \frac{1}{2}\int_0^{t_f} \sum_i \left(\frac{dT_i}{dt}\right)^2 dt, \tag{6}$$

which is the time integral of the squared sum of the rate of change in muscle tension. Here, T_i expresses the tension generated by the ith muscle. To reduce the dynamic redundancy, we proposed a feedback control law related to the minimum-muscle-tension-change criterion (Katayama and Kawato, 1991a), which is applied to the feedback controller shown in Fig. 1. An inverse of the Jacobian matrix calculating from small changes in muscle tensions to small changes in joint torques is not uniquely determined because the matrix is not a square. However, by using the pseudo-inverse matrix (the Moore-Penrose generalized inverse matrix) of the Jacobian matrix, small changes in muscle tension can be uniquely determined from small changes in joint torque. The solution is based on instantaneous minimization of the muscle tension change because the Euclidean norm of small changes in muscle tension is minimized by the pseudo-inverse matrix. Necessary changes in joint torque are first calculated by a simple feedback control law such as a PID (proportional, integral and derivative) controller from the difference between actual and desired trajectories. Then, by applying the pseudo-inverse matrix, small changes in muscle tensions are uniquely calculated. Combination of this feedback control law and the feedback-error-learning can solve dynamic redundancy. Learning is performed by applying the feedback motor command u_{fc} to the learning algorithm (5). As a result, inverse statics and dynamics models, based approximately on the minimum-muscle-tension-change model, can be acquired. We ascertained the efficiency of the parallel-hierarchical neural network model in learning control experiments using an artificial muscle arm with agonist and antagonist muscle-like rubber actuators driven by air and made by Bridgestone Co., Ltd. (Katayama and Kawato, 1991a).

3. Arm modelling

Insert Figure 3 around here

3.1 Muscle modelling

One of the most important properties of muscles is to change their visco-elasticity according to their activation level. Realistic muscle models including many elastic and viscous elements have been proposed, but, when modeling the human arm, it is difficult to determine many parameters in such a model. We therefore used a simpler model consisting of an elastic element and a viscous element connected in parallel, since the parameters in the simpler model can be determined from previous studies. This model is called the Kelvin-Voight model (Özkaya, Nordin, 1991). The muscle tension T is mathematically described as

$$T(l,\dot{l},u) = K(u)\{l_r(u) - l\} - B(u)\dot{l} \qquad (7)$$

Here l is the muscle length vector and $\dot{l}$ is the contraction velocity vector. $K(u)$, $B(u)$ and $l_r(u)$ express muscle stiffness, muscle viscosity and rest length of the muscle. They depend nonlinearly on the motor command u e.g., motoneuronal activations (see Fig. 2B). We assume, however, that $K(u)$, $B(u)$, and $l_r(u)$ have the following linear dependencies on the motor command u:

$$K(u) = k_0 + ku \qquad (8a)$$

$$B(u) = b_0 + bu \qquad (8b)$$

$$l_r(u) = l_0 + ru \tag{8c}$$

Here k and b are the elasticity and viscosity coefficients, respectively, and k_0 and b_0 are the intrinsic elasticity and viscosity. The term l_0 is the intrinsic rest length when u is zero, and r is a constant.

3.2 2-link arm model with 6 muscles

It is suggested that double-joint muscles play an important role in arm movement and force control (Hogan, 1985; Flash and Mussa-Ivaldi, 1990; Tsuji, Ito, Nagamachi, Ikemoto, 1988). In this paper, the human arm is modeled as a 2-link manipulator with four single-joint muscles and two double-joint muscles (Fig. 3). Since the 2-link manipulator has no kinematic redundancy, the inverse kinematics problem can be solved uniquely.

The muscle tension vector $T(l,\dot{l},u)$ and the moment arm matrix $A(\theta)$ are described as follows:

$$T(l,\dot{l},u) = (T_1,T_2,T_3,T_4,T_5,T_6)^T, \tag{9a}$$

$$A(\theta) = \begin{pmatrix} a_1(\theta_s) & a_2(\theta_s) & 0 & 0 & a_5(\theta_s) & a_6(\theta_s) \\ 0 & 0 & a_3(\theta_e) & a_4(\theta_e) & a_7(\theta_e) & a_8(\theta_e) \end{pmatrix}^T. \tag{9b}$$

The subscripts s and e express shoulder and elbow joints. T_1 and T_2 are the respective tensions of the shoulder flexor and extensor, T_3 and T_4 are those of the elbow flexor and extensor, and T_5 and T_6 are those of the double-joint flexor and extensor. The overall joint torque vector, $\tau(\theta,\dot{\theta},u)$, is calculated from (2b) and consists of the shoulder joint torque τ_s and the elbow joint torque τ_e. By assuming constant moment arms that do not depend on joint angles, $A(\theta) = A$, the muscle length vector is given as

$$l = l_m - A\theta. \tag{10}$$

Here the joint angle vector θ consists of θ_s and θ_e, l_m is the muscle length when the joint angle θ is zero. The joint stiffness R and viscosity D are then derived as

$$R = \frac{\partial \tau}{\partial \theta} = A^T \frac{\partial T}{\partial l}\frac{\partial l}{\partial \theta} = A^T K(u) A, \tag{11a}$$

$$D = \frac{\partial \tau}{\partial \dot{\theta}} = A^T \frac{\partial T}{\partial \dot{l}}\frac{\partial \dot{l}}{\partial \dot{\theta}} = A^T B(u) A. \tag{11b}$$

The joint stiffness and viscosity matrices here are symmetrical. The dynamics equation of a planar 2-joint arm is thus given as

$$\begin{pmatrix} I_1+I_2+2M_2L_1L_{g2}\cos(\theta_e)+M_2L_1^2 & I_2+M_2L_1L_{g2}\cos(\theta_e) \\ I_2+M_2L_1L_{g2}\cos(\theta_e) & I_2 \end{pmatrix}\begin{pmatrix} \ddot{\theta}_s \\ \ddot{\theta}_e \end{pmatrix}$$
$$+M_2L_1L_{g2}\sin(\theta_e)\begin{pmatrix} -2\dot{\theta}_e & -\dot{\theta}_e \\ \dot{\theta}_s & 0 \end{pmatrix}\begin{pmatrix} \dot{\theta}_s \\ \dot{\theta}_e \end{pmatrix}=\begin{pmatrix} \tau_s \\ \tau_e \end{pmatrix} \quad . \quad (12)$$

The subscripts 1 and 2 respectively indicate the upper arm and the forearm. I is the moment of inertia around the joint, L is the link length, L_g is the center of gravity of each link, M is the link weight.

3.3 Arm model physical parameters

3.3.1 Arm parameters

Insert Table 1 around here
Insert Table 2 around here

The physical parameters of a 2-link arm are estimated from previous measurements. Morasso (1981) measured the length of the humerus and the forearm in adult subjects and found that the difference between the lengths of the humerus and the forearm, ranged from 0 to 10 cm. In the present paper it is assumed that the upper arm is 30 cm long and the forearm is 35 cm long. The weights of the two links estimated in previous studies are used, and the moment of inertia around the joint is calculated from the length and weight of each link. The center of gravity for each link is determined according to Hatze's suggestions (Hatze, 1979). These parameters are listed in Table 1. Amis, Dowson, Wright (1979) examined the moment arms for each muscle around the elbow joint and found a nonlinear relationship between the moment arm and the joint angle. In this paper, however, we assumed constant-moment arms (Table 2) described by the average values of anatomical data (Amis et al., 1979; Wood, Meek, Jacobsen, 1989a, 1989b).

3.3.2 Muscle parameters

Insert Table 3 around here

Physical properties such as stiffness and viscosity are known to include the combined influence of muscle intrinsic properties and low-level neural feedback. The stiffness value of individual muscle measured *in vitro* does not include the influence of neural reflexes (Rack and Westbury, 1974). Moreover, the complexity of neural-musculoskeletal system makes it difficult to predict the joint or hand stiffness from the muscle stiffness. Elbow joint stiffness has been experimentally measured *in vivo* with small perturbations (Lacquaniti, Licata, Soechting, 1982; MacKay, Crammond, Kwan, Murphy, 1986) by using a linear second-order model of motor system. MacKay et al. found that the elbow stiffness values measured in different subjects ranged from 2 to 12 N-m/rad, the elbow viscosity values ranged from 0.1 to 0.2 N-m-sec/rad, and the joint stiffness and viscosity depended on the joint angle. As described in section 1, Mussa-Ivaldi et al. (1985) characterized the field of elastic forces as a stiffness ellipse. The measured hand stiffness ranged from about 100 to 450 N/m and the elbow stiffness which was estimated from the hand stiffness ranged from about 10 to 40 N-m/rad. The measurements and analysis methods in previous studies were different, and the measured stiffness values therefore also differed considerably. The main reasons for the variation seem to be the coactivation of agonist and antagonist muscles and the phasic and tonic properties in neural reflexes and muscle responses. The phasic properties and the coactivation induce higher joint stiffness. For example, the stiffness increases as the amplitude of instantaneous changes in displacement decreases (Rack and Westbury, 1974; MacKay et al., 1986). The coactivation caused by gripping a handle may exist in Mussa-Ivaldi's experiment because some muscles activated for hand grasp are multi-joint muscles connected to the humerus. Some of the stiffness values measured in previous studies may therefore be larger than the true, at-rest stiffness values.

Moreover, the dynamic stiffness during movement may be quite different from the at-rest stiffness during posture maintenance, because the activation level of the neural reflexes during fast movements may be suppressed by descending signals from the CNS. Bennett, Hollerbach, Xu, Hunter (1992) measured elbow joint mechanical impedance (stiffness, viscosity, and moment of inertia) during a single-joint cyclic movement at an amplitude of 1 radian with a period of 750 msec. In this experiment, small pseudo-random force disturbances were applied to the wrist with an airjet actuator. The mechanical impedance was estimated by an autoregressive moving average model (ARMA) using a quasi-linear second-order model of the single-joint motor system. As a result, they found that the elbow stiffness values during the cyclic movement were smaller than the at-rest stiffness during posture maintenance. In a related experiment, Bennett (1991) measured joint stiffness values during the elbow joint movement by using a powerful direct-drive motor to apply positional perturbations and then to measure the resulting torques. Although the two methods differed, the estimated stiffness values during movement were similar. Additionally, he found that the at-rest elbow stiffness values ranged from 3 to 5 N-m/rad and that the at-rest stiffness during posture maintenance was smaller than the dynamic stiffness during movements. The at-rest stiffness values were also about 50-12.5% smaller than those measured by Mussa-Ivaldi et al. (1985) and Bennett et al. (1992). We therefore used the dynamic elbow stiffness and viscosity values measured by Bennett et al. (1991, 1992). The measured stiffness and viscosity values changed somewhat independently (Bennett et al., 1992). The stiffness ranged from 2 to 9 N-m/rad and the viscosity ranged from 0 to 0.7 N-m-sec/rad. We roughly determined the elbow stiffness and viscosity coefficients by considering only the maximum and minimum values of these measured parameters, assuming that the muscle stiffness and viscosity values are proportional to the motor command, as described in (8). Because a value of 0 is implausible for the minimum viscosity, we assumed a value of 0.2 N-m-sec/rad. Consequently, the damping ratio of the forearm, calculated as $D_{22} / \sqrt{4M_{22}R_{22}}$, was 0.24 when all the motor commands were zero.

Flash and Mussa-Ivaldi (1990) showed that the necessary and sufficient condition for the major axis of the stiffness ellipse pointing towards the shoulder is that the single-joint shoulder muscle stiffness is equal to the two-joint muscle stiffness. In our human arm model, the stiffness and viscosity values are minimal at a functional standard posture where all motor commands are zero. In this paper, the functional standard posture is defined as that where the shoulder joint angle is 45 degrees and the elbow joint angle is 70 degrees. Roughly speaking, the ratio of the shoulder and elbow stiffness measured by Flash and Mussa-Ivaldi (1990) around the functional standard posture matches the ratio calculated when assuming that the six muscle stiffness values are all the same. We therefore assumed that all the stiffness values of six muscles are the same and that all the viscosity values are also the same. Using this assumption, we calculated the shoulder and elbow joint stiffness from these muscle stiffnesses and their moment arms, as described in Eqs. (11a) and (11b). The joint stiffness and viscosity values at the functional standard posture were estimated as

$$R_{standard} = \begin{pmatrix} \frac{\partial \tau_s}{\partial \theta_s} & \frac{\partial \tau_s}{\partial \theta_e} \\ \frac{\partial \tau_e}{\partial \theta_s} & \frac{\partial \tau_e}{\partial \theta_e} \end{pmatrix} = \begin{pmatrix} 3.9 & 1.6 \\ 1.6 & 3.0 \end{pmatrix} \quad N \cdot m / rad,$$

$$D_{standard} = \begin{pmatrix} \frac{\partial \tau_s}{\partial \dot{\theta}_s} & \frac{\partial \tau_s}{\partial \dot{\theta}_e} \\ \frac{\partial \tau_e}{\partial \dot{\theta}_s} & \frac{\partial \tau_e}{\partial \dot{\theta}_e} \end{pmatrix} = \begin{pmatrix} 0.26 & 0.11 \\ 0.11 & 0.20 \end{pmatrix} \quad N \cdot m \cdot \sec / rad.$$

Note that these joint stiffness and viscosity values are smallest for the standard posture. The coefficient r was roughly determined from the isometric length-tension curves measured by Rack and Westbury (1969). The values of $l_m - l_0$ were chosen so as to fit the defined functional standard posture. All the muscle parameters are listed in Table 3. With these parameters, the damping ratio increases as the motor commands increase.

4. Prediction of virtual trajectory and stiffness ellipse

4.1 Dynamic stiffness

In this section, we introduce the definition of dynamic stiffness during movement. Dynamics equations in the Cartesian coordinates can generally be expressed as

$$\phi(x, \dot{x}, \ddot{x}, u) = 0. \qquad (13)$$

Here x is the position and u is the motor command. Let us assume that the velocity, acceleration, and motor commands do not change during perturbed movement when instantaneous small changes in displacement occur at a given time t. The dynamic stiffness can thus be defined as

$$Dynamic\ stiffness(t) = \frac{\partial}{\partial x}\phi(x,\dot{x},\ddot{x},u) \quad (14)$$

This is the definition of the dynamic stiffness. The dynamics equation for a multi-joint arm movement can be described in the joint coordinates as

$$\varphi(\theta,\dot{\theta},\ddot{\theta},u) = M(\theta)\ddot{\theta} + C(\theta,\dot{\theta})\dot{\theta} + G(\theta) - \tau(\theta,\dot{\theta},u) = 0 \quad (15)$$

The restoring torque $\delta\varphi$ caused by small changes in displacement $\delta\theta$ is

$$\delta\varphi = \frac{\partial\varphi(\theta,\dot{\theta},\ddot{\theta},u)}{\partial\theta}\delta\theta \quad (16)$$

The restoring torque is translated to the hand force δF by using an inverse of the Jacobian transpose:

$$\delta F = \left(J^T\right)^{-1}\delta\varphi \quad (17)$$

As a result, the four hand-stiffness coefficients of S are uniquely calculated from torque responses to positional perturbations in two different directions:

$$\delta x = J\delta\theta \quad (18a)$$

$$\delta F = S\delta x \quad (18b)$$

This definition of the dynamic hand stiffness corresponds to the hand stiffness measured experimentally with small positional perturbations (Gomi, Koike, Kawato, 1992), but in most cases it is in fact necessary to consider the influence of the small changes in velocity and acceleration caused by the perturbations (MacKay et al., 1986; Lacquaniti et al., 1982; Bennett et al., 1992; Gomi et al., 1992).

Here we introduce another possible definition of dynamic stiffness which is more appropriate for virtual trajectory control hypothesis. We believe the hand stiffness S in (1) should be derived from the joint stiffness $\partial\tau / \partial\theta$ caused by the muscles themselves because in the virtual trajectory control the dynamic forces (e.g., inertia and Coriolis forces) act as external forces. The hand stiffness is therefore calculated by using Eqs. (17), (18), and the following equation:

$$\delta\varphi = \left(-\frac{\partial\tau}{\partial\theta}\right)\delta\theta \quad (19)$$

The hand stiffness matrices can be represented graphically as ellipses by using the following equation (Mussa-Ivaldi et al., 1985).

$$\begin{pmatrix} x_f \\ y_f \end{pmatrix} = \begin{pmatrix} x \\ y \end{pmatrix} + \alpha \begin{pmatrix} S_{xx} & S_{xy} \\ S_{yx} & S_{yy} \end{pmatrix} \begin{pmatrix} \cos(t) \\ \sin(t) \end{pmatrix} \quad (20)$$

$$(0 \le t < 2\pi)$$

Here, (x_f, y_f) is a position on ellipse, (x, y) is a concurrent position, and α is a scaling coefficient.

4.2 Virtual trajectory

If the motor command *u(t)* at time *t* is kept constant for an infinite time, the equilibrium posture should be observed. When the motor commands u are given to muscles at time t, the virtual trajectory, represented by the virtual joint angle θ_V or the virtual muscle length l_V, can be derived from the following equilibrium condition.

$$A^T T(l_V, 0, u) = 0 \quad (21)$$

Here the virtual joint trajectory θ_V is calculated by putting l_V into (10). Eq. (21) is the same form as the statics equation (3) in planar movements. However, the motor commands used in (3) and (21) are different. The motor command u in (3) specifies the equilibrium posture, while the u in (21) is the motor command during movement at time t. The virtual trajectory X_V in the hand coordinates is translated from the joint coordinates using a forward kinematics equation $L(\theta)$, as

$$X_V = L(\theta_V) \quad (22)$$

5. Simulation results

5.1 Stiffness ellipses during posture maintenance

The inverse statics model ISM was first trained during posture control. The ISM was structured as a three-layer perceptron with 2-30-6 neuron units. The ISM learning required about 10,000 iterations. As shown in Fig. 4, the orientation and shape of the predicted stiffness ellipses were similar to those measured by Mussa-Ivaldi et al. (1985). The shape narrowed as the hand approached the work-space boundary, and the stiffness ellipses were oriented with the major axis roughly pointing towards the shoulder. The major axis of the stiffness ellipse gradually turned towards the elbow as the hand approached the body. Note that the hand stiffness values measured by Mussa-Ivaldi were about six to ten times larger than those estimated by our simulation. This is because we used the low stiffness values measured by Bennett et al. (1991, 1992) in this simulation. When only the single-joint muscles were used in a human arm model, the shape of the stiffness ellipses became overly narrow (Katayama and Kawato, 1991b).

Insert Figure 4 around here

5.2 Virtual trajectories and stiffness ellipses during movement

----

Insert Figure 5 around here

We first simulated single-joint forearm movement. A single-joint dynamics equation was used, the shoulder joint angle was fixed, and two elbow-joint muscles and two double-joint muscles were used. The virtual trajectories for single-joint movement were predicted. The virtual trajectories were similar to those simulated by Hogan (1984) and were as simple as the desired or actual trajectories. The elbow joint stiffness values ranged from 3.0 to 3.9 N-m/rad in a discrete movement at 1-radian amplitude with 750-msec duration. This dynamic range was smaller than that measured for similar cyclic movements by Bennett et al. (1992).

Accordingly, the parallel-hierarchical neural network model was used to train the inverse statics and dynamics models for each movement. The IDM was a three-layer perceptron with 6-30-6 neuron units. The IDM learning was performed by using trained ISM. The learning iteration number was about 5,000. The desired trajectories between the targets were determined as the minimum-jerk trajectory (Flash and Hogan, 1985). The target locations are shown in Fig. 5. Learning trajectory control was carried out for each movement: T2-T6, T2-T5, T3-T6, and T4-T1. These movements were performed with two movement durations: 500 and 750 msec. After both inverse models are trained, the stiffness ellipses during each movement were predicted from (18), (19), and (20) and the virtual trajectories were predicted from (21) and (22). The predicted stiffness ellipses during movement are shown in Fig. 6. Note that the predicted stiffnesses do not involve the influence of the terms M, C, and G in (15), as mentioned in section 4.1. For fast movements, the orientation, size, and shape of the ellipses changed markedly because the IDM outputs changed during movement. These characteristics depended on the orientation, position, amplitude, and speed of the movement. The dynamic stiffness matrices during movements are not generally symmetrical. The predicted dynamic hand stiffness matrices were, however, almost symmetrical for 500-msec and 750-msec point-to-point movements.

Fig. 7 shows the desired, actual, and virtual trajectories for each movement, and also shows the tangential velocity profiles corresponding to these three kinds of trajectories. Because the IDM learning was not perfect, the difference between the desired and actual trajectories was observed and the velocity values of the virtual trajectories were not zero around the initial and final positions. For fast movements, the predicted virtual trajectories were curved and much more complex than the actual trajectories. This is because of the larger dynamic forces of the 2-link manipulator, and spatial anisotropies of the stiffness ellipses. For slow movements, however, the virtual trajectories are more similar to the actual trajectories. The minimum-jerk point-to-point trajectories have a bell-shaped tangential velocity profile, but some of the virtual trajectories have tangential velocity profiles with two more peaks. Moreover, Figure 8, which shows the actual and virtual trajectories in the joint coordinates, indicates that the trajectories were as complex as the virtual trajectories represented in the Cartesian coordinates. These results indicate that it is not easy to plan the virtual trajectory either in the task or joint coordinates. Virtual trajectory planning therefore appears to be as complex as solving the inverse dynamics problem.

The motor commands to six muscles during T2-T6 750-msec movement are shown in Fig. 9. For 750-msec movements, the dynamic joint stiffness coefficients were less than 1.3 times the at-rest joint stiffness. For the T2-T6 trajectory, the element R_{11} of the dynamic joint stiffness ranged from 4.4 to 5.6 N-m/rad, R_{22} ranged from 3.5 to 4.4 N-m/rad, R_{12} and R_{21} ranged from 1.7 to 2.3 N-m/rad, and the damping ratio of the forearm ranged from 0.26 to 0.29. The element S_{xx} of the dynamic hand stiffness ranged from 14 to 65 N/m, S_{yy} ranged from 40 to 64 N/m, S_{xy} and S_{yx} ranged from -7 to 29 N/m. For 500-msec movements, the dynamic joint stiffness coefficients were less than 1.5 times the at-rest joint stiffness. For the T2-T6 trajectory, the element R_{11} of the dynamic joint stiffness ranged from 4.2 to 6.7 N-m/rad, R_{22} ranged from 3.6 to 4.6 N-m/rad, R_{12} and R_{21} ranged from 1.8 to 2.3 N-m/rad, and the damping ratio of the forearm ranged from 0.26 to 0.3. The element S_{xx} of the dynamic hand stiffness ranged from -13 to 80 N/m, S_{yy} ranged from 40 to 97 N/m, S_{xy} and S_{yx} ranged from -27 to 52 N/m. For the static hand stiffness during posture maintenance along the T2-T6 trajectory, S_{xx} ranged from 25 to 63 N/m, S_{yy} ranged from 35 to 71 N/m, S_{xy} and S_{yx} ranged from -10 to 16 N/m. We found that some of the dynamic stiffnesses during movement were smaller than the at-rest stiffnesses during posture maintenance. This is because some of the motor commands, which are the sum of the ISM and IDM outputs, are smaller than the ISM outputs required to maintain the posture at time *t*, as shown in Fig. 9.

Insert Figure 6 around here
Insert Figure 7 around here
Insert Figure 8 around here
Insert Figure 9 around here

We also examined simulation results whenever we assumed different stiffness and viscosity values. As mentioned before, the simulated dynamic range of the elbow stiffness values was smaller than the dynamic range measured by Bennett (1992). The elbow stiffness and viscosity values were determined as the average of the values during cyclic movement (Bennett, 1992). That is,

$$R_{standard} = \begin{pmatrix} 6.4 & 2.7 \\ 2.7 & 5.0 \end{pmatrix} \quad N \cdot m / rad \; ,$$

$$D_{standard} = \begin{pmatrix} 0.45 & 0.19 \\ 0.19 & 0.35 \end{pmatrix} \quad N \cdot m \cdot \sec / rad \; .$$

These are values at the functional standard posture. Consequently, the damping ratio of the forearm was 0.32. For the single-joint discrete movement at 1-radian amplitude with 750-msec duration, the elbow stiffness values simulated ranged from 5.0 to 6.4 N-m/rad. The virtual trajectories for T2-T6 two-joint movements are shown in Fig. 10. The predicted virtual trajectories were more complex than the desired trajectories, although the predicted virtual trajectories were simpler than those shown in Fig. 7, because of comparatively larger stiffness values. For the 500-msec movement, the dynamic elbow stiffness values ranged from 5.7 to 7.3 N-m/rad, the shoulder stiffness from 7.0 to 10.1 N-m/rad, and the damping ratio of the forearm from 0.35 to 0.42.

Finally, even larger stiffness values at the functional standard posture were examined. The stiffness value was determined from those measured by Mussa-Ivaldi et al. (1985) during posture maintenance, and the viscosity values were determined so that damping ratio of the forearm was 0.24.

$$R_{standard} = \begin{pmatrix} 21.6 & 8.9 \\ 8.9 & 16.8 \end{pmatrix} \quad N \cdot m / rad \; ,$$

$$D_{standard} = \begin{pmatrix} 0.61 & 0.25 \\ 0.25 & 0.47 \end{pmatrix} \quad N \cdot m \cdot \sec / rad \; .$$

The virtual trajectories are shown in Fig. 11. Using larger stiffness values, the predicted virtual trajectories became simpler, but the virtual trajectories for ballistic 250-msec movements were much more complex than the actual trajectories. Thus, the virtual trajectories become simple as the stiffness values increase.

Insert Figure 10 around here

Insert Figure 11 around here

5.3 ISM control

We tried ISM control using straight desired trajectories based on the minimum-jerk model (Flash and Hogan, 1985), which is similar to Flash's simulation (Flash, 1987). Trajectory control was performed by only the ISM inputting the minimum-jerk trajectory. The trajectories produced by ISM control are shown in Fig. 12. Here, only the generated hand paths during the specified movement durations (750ms or 500ms) are shown. The virtual trajectories used in ISM control is exactly the same as the desired trajectories. For slow T2-T6 movements, the actual trajectories seem similar to human subject data because the T2-T6 human arm trajectory is distally curved a little. The simulated actual T4-T1 trajectories for example, however, differed from the human arm trajectories because the T4-T1 human arm trajectory is almost straight. For faster movements, the actual trajectories varied more. These results differed from Flash's simulation results because the stiffness values used in this simulation were smaller than those assumed by Flash (1987).

Insert Figure 12 around here

----

6. Discussion

This paper investigated the virtual trajectories and stiffness ellipses predicted by the learned inverse statics and dynamics models. The predicted virtual trajectories for faster point-to-point movements were curved, and much more complex than the actual trajectories. Thus, we found that planning the virtual trajectories is not easy, and appears to be as complex as solving the inverse dynamics problem. However, we must note that this conclusion heavily depends on several assumptions made in this study. First, as can be seen by comparing Figs. 7, 10, and 11, virtual trajectory profiles are quite dependent on the assumed stiffness values during movement. Thus, it is important to exactly estimate the muscle physical parameters during posture maintenance and movement, but reliable estimation seems rather difficult. Second, how to determine the motor commands is not at all apparent. The simulated coactivation of pairs of muscles was quite small because instantaneous minimization of muscle-tension change was adopted in this study.

Flash's simulation results (1987) differed from ours even for relatively slow movements. The differences can be readily understood if one recalls that the required joint torques are generated as the product of the mechanical stiffness and the difference between the virtual and actual trajectories. If physical parameters such as inertia moments, masses, and lengths of links are given and the actual hand trajectory is fixed, the required joint torques are uniquely determined from the inverse dynamics equation. When the stiffness is small, this difference becomes large. Human multi-joint hand paths are roughly straight for point-to-point movements. Consequently, in Flash's simulation, and assuming relatively high stiffness values, the virtual trajectory could be close to the human arm trajectory. For T2-T6 movement, Flash (1987) assumed that the R_{11}, R_{12}, and R_{22} of the dynamic joint stiffness matrix during 1-second movement are 80.7, 42.9, and 68.9 N-m/rad, respectively. Moreover, Flash (1987) assumed a wide damping ratio range during the movements: 0.35 to 1.5. The damping ratio was larger than those used in our simulation. However, previous measurements indicated that the human arm is an underdamped system (Bennett, 1992; MacKay et al., 1986; Lacquaniti et al., 1982). The virtual trajectories predicted by using an arm model that roughly approximates a critically-damped system were also more complex than the actual trajectories, although the profiles differed from those shown in Figs. 7, 10, and 11 (Katayama and Kawato, 1991b).

Relatively low stiffness values were assumed in our simulation. For T2-T6 movement, the R_{11}, R_{12}, and R_{22} of the dynamic joint stiffness matrix during 750-msec movement averaged 5.1, 2.0, and 3.9 N-m/rad, respectively. These values were about 2.5-5% smaller than those assumed by Flash (1987). Thus, the virtual trajectory was very different from the actual trajectory and was wildly curved. If actual stiffness during movement is relatively small, then to achieve the roughly straight hand paths observed, the virtual trajectory must be planned carefully to compensate for the dynamic link interaction forces between arm segments. This planning problem is nearly equivalent to solving the inverse dynamics problem and is similarly difficult. For slow movements, however, virtual trajectory control is quite effective. Jordan (1990) proposed a neural network model to train the virtual trajectory for single-joint movements. This is a possible strategy to combine the virtual trajectory control hypothesis with the internal models.

For posture control, the orientation and shape of the predicted stiffness ellipses were similar to those measured by Mussa-Ivaldi et al. (1985). For single-joint movement, however the dynamic range of the stiffness during movement was smaller than the dynamic range estimated by Bennett et al. (1992). This might be partly because of the difference between the point-to-point movements studied here and the cyclic movements studied by Bennett. In Bennett's experiment, the coactivation of pairs of muscles may have occurred just before reaching targets during cyclic movement. On the other hand, the adopted instantaneous minimization of the muscle-tension-change did not reproduce such coactivation because quite small motor commands were selected. The minimum-muscle-tension-change criterion is effective from the standpoint of energy consumption in muscles, while the postures and movements may be more stably controlled when the control system uses coactivation. We need to further examine how to explain such a coactivation mechanism. One possible strategy would be to use a learning control model based on the minimum-motor-command-change model (Kawato, 1992) rather than the minimum-muscle-tension-change model, because the feedback control law related to the *minimum-motor-command-change* model can explain the coactivation of a pair of muscles (Katayama and Kawato, 1991a).

We found that some of the dynamic stiffness values were smaller than the static stiffness during posture maintenance, as mentioned above. Bennett et al. (1992) found that the elbow stiffness values during cyclic movement were smaller than the at-rest stiffness during posture control. Moreover, Gomi, Koike, and Kawato (1992) recently measured the time-varying stiffness of a multi-joint arm during discrete point-to-point movements rather than single-joint movement and found that some of the dynamic stiffness values were smaller than the static stiffness during posture maintenance. This is possibly because, during fast movement, the activation level of the low-level neural reflexes might be suppressed by the descending signals, and the motor command values during movements might be smaller than those required to maintain the posture. Moreover, in Gomi's experiment during T2-T6 750-msec movement, the hand stiffness value S_{yy} ranged from 50 to 200 N/m. The hand stiffness values estimated in this simulation during such a movement were within this measured hand stiffness value range. With this in mind, such experimental findings may support our assumptions and conclusion.

In this paper, we presented the various virtual trajectories predicted by using the stiffness values of three cases where the elbow joint stiffness values are 3.0, 5.0, and 16.8 N-m/rad. For point-to-point trajectory control using relatively small stiffness values range from 3.0 to 5.0 N-m/rad, the complicated virtual trajectories were predicted, while using a relatively large stiffness value of 16.8 N-m/rad resulted in simpler virtual trajectories. Consequently, when the human elbow stiffness values are less than about 15 N-m/rad, it is essential to solve the inverse dynamics problem or to plan the complicated virtual trajectories by training the internal models of the motor systems. In contrast, when the human elbow stiffness values are larger than about 15 N-m/rad, even a simpler control mechanism such as the virtual trajectory control hypothesis can explain the feedforward arm control. Based on these considerations, we finally propose an integrated computational scheme which is based both on the virtual trajectory control hypothesis and learning inverse internal models. Fig. 13 shows the architecture of the integrated model. The VTP (Virtual Trajectory Planner) stands for the internal inverse model which calculates the virtual trajectory form the desired trajectory. Several advantages of this scheme can be pointed out. First the VTP could be a unity function for slow movements or high stiffness conditions. Thus the CNS can start learning movement with slow movement conditions or high stiffness conditions, then adapt VTP to fast movements with low stiffness (see related work by Sanger, 1992). Second, as the input and the output of the VTP are represented in the same Cartesian coordinates, it is quite straightforward to design the feedback controller (FC in Fig. 13), which is the most difficult part of the feedback-error-learning. It is one of our future projects to examine the computational efficiency and biological plausibility of this integrated scheme.

Acknowledgments

We are grateful to Drs. Masaaki Sato, Yasuhiro Wada, Menashe Dornay, Yasuharu Koike, Hiroaki Gomi, David Bennett, and Terry Sanger for their helpful comments and discussions during preparation of this manuscript. This work was supported by a Human Frontier Science Program Grant to M. Kawato.

References

Abend, W., Bizzi, E., Morasso, P.: Human arm trajectory formation. Brain **105**, 331-348 (1982).

Amis, A.A., Dowson, D., Wright, V.: Muscle strengths and musculoskeletal geometry of the upper limb. Engineering in Medicine **8**, 1, 41-48 (1979).

Atkeson, C.G., Hollerbach, J.M.: Kinematic features of unrestrained vertical arm movement. Journal of Neuroscience **5**, 2318-2330 (1985).

Bennett, D.J.: Relationship between stiffness and net joint torque during ballistic elbow joint movement. Society for Neuroscience Abstracts **17**, 1029 (1991).

Bennett, D.J., Hollerbach, J.M., Xu, Y., Hunter, I.W.: Time-varying stiffness of human elbow joint during cyclic voluntary movement. Experimental Brain Research **88**, 433-442 (1992).

Bizzi, E., Polit, A., Morasso, P.: Mechanism underlying achievement of final head position. J. Neurophysiol. **39**, 435-444 (1976).

Bizzi, E., Accornero, N., Chapple, W., Hogan, N.: Posture control and trajectory formation during arm movement. The Journal of Neuroscience **4**, 11, 2738-2744 (1984).

Fel'dman, A. G.: Functional tuning of the nervous system with control of movement or maintenance of a steady posture. III. Mechanographic analysis of execution by man of the simplest motor tasks. Biophysics 11, 766-775 (1966).

Fel"dman, A. G., Adamovich, S. V., Ostry, D.J., Flanagan, J. R.: The origin of electromyograms-Explanations based on the equilibrium point hypothesis. In Multiple Muscle Systems: Biomechanics and Movement Organization. Winters, J.M., Woo, S.L-Y. (Eds), Springer-Verlag, New York (1990).

Flash, T., Hogan, N.: The coordination of arm movements: an experimentally confirmed mathematical model. The Journal of Neuroscience **5**, 7, 1688-1703 (1985).

Flash, T.: The control of hand equilibrium trajectories in multi-joint arm movement. Biological Cybernetics **57**, 257-274 (1987).

Flash, T., Mussa-Ivaldi, F. A.: Human arm stiffness characteristics during the maintenance of posture. Experimental Brain Research **82**, 315-326 (1990).

Gomi, H., Kawato, M.: Learning control for a closed loop system using feedback-error-learning. Proc. the 29th IEEE Conference on Decision and Control, Hawaii, 3289-3294 (1990).

Gomi, H., Koike, Y., Kawato, M.: Human hand stiffness during discrete point-to-point multi-joint movement. Proc. IEEE EMBS (1992) submitted.

Hatze, H.: A model for the computational determination of parameter values of anthropomorphic segments. National research Institute for Mathematical Sciences, CSIR, South Africa, Technical report TWISK 79 (1979).

Hogan, N.: An organizing principle for a class of voluntary movements. The Journal of Neuroscience **4**, 11, 2745-2754 (1984).

Hogan, N.: The mechanics of multi-joint posture and movement control. Biological Cybernetics **52**, 315-331 (1985).

Ito, M.: Neurophysiological aspects of the cerebellar motor control system. Int. J. Neurol. **7**, 162-176 (1970).

Jordan, M.I.: Motor learning and the degrees of freedom problem. In M. Jeannerod (Ed.), Attention and Performance XIII (pp.796-836). Hillsdale: Lawrence Erlbaum Associates.(1990)

Katayama, M., Kawato, M.: Parallel-hierarchical neural network model for motor control of musculoskeletal system. Systems and Computers in Japan, Scripta Technica, Inc., **22**, 6, 95-105 (1991a).

Katayama, M., Kawato, M.: Virtual trajectory and stiffness ellipse during force-trajectory control using a parallel-hierarchical neural network model. Fifth International Conference on Advanced Robotics, 1187-1194 (1991b).

Kawato, M., Furukawa, K., Suzuki, R.: A hierarchical neural-network model for control and learning of voluntary movement. Biological Cybernetics **57**, 169-185 (1987).

Kawato, M.: Optimization and learning in neural networks for formation and control of coordinated movement. In Meyer D, Kornblum S (eds) Attention and Performance, XIV: Synergies in Experimental Psychology, Artificial Intelligence, and Cognitive Neuroscience - a Silver Jubilee. MIT Press, Cambridge, Massachusetts, in press.

Lacquaniti, F., Licata, F., Soeching, J.F.: The mechanical behavior of the human forearm in response to transient perturbations. Biological Cybernetics **44**, 35-46 (1982).

MacKay, W.A., Crammond, D.J., Kwan, H.C., Murphy, J.T.: Measurements of human forearm viscoelasticity. Journal of Biomechanics **19**, 3, 231-238 (1986).

Morasso, P.: Spatial control of arm movements. Experimental Brain Research **42**, 223-227 (1981).

Mussa-Ivaldi, F. A., Hogan, N., Bizzi, E.: Neural, mechanical, and geometric factors subserving arm posture in humans. The Journal of Neuroscience **5**, 10, 2732-2742 (1985).

Özkaya, N., Nordin, M.: Fundamentals of biomechanics: equilibrium, motion, and deformation. Van Nostrand Reinhold, New York (1991).

Polit, A., Bizzi, E.: Characteristics of the motor programs underlying arm movements in monkeys. J. Neurophysiol. **42**, 183-194 (1979).

Rack, P.M.H., Westbury, D.R.: The effects of length and stimulus rate on tension in the isometric cat soleus muscle. Journal of Physiology **217**, 419-444 (1969).

Rumelhart, D.E., Hinton, G.E., Williams, R.J.: Learning representations by back-propagating errors. Nature **323**, 533-536 (1986).

Sanger, T: Learning inverse dynamics by local exploration. Abstract for Neural Networks for Computing Snowbird, (1992).

Tsuji, T., Ito, K., Nagamachi, M., Ikemoto, T.: Impedance regulations in musculo-motor control system and the manipulation ability of the end-point. SICE **24**, 4, 385-392 (1988) in Japanese.

Tsukahara, N., Kawato, M.: Dynamic and plastic properties of the brain stem neuronal networks as the possible neuronal basis of learning and memory. Competition and cooperation in neural nets, Amari, S., Arbib, M.A. (Eds), New York: Springer-Verlag, 430-441 (1982).

Uno, Y., Kawato, M., Suzuki, R.: Formation and control of optimal trajectory in human multijoint arm movement: minimum-torque-change model. Biological Cybernetics **61**, 89-101 (1989a).

Uno, Y., Suzuki, R., Kawato, M.: Minimum-muscle-tension-change model which reproduces human arm movement. Proceedings of the 4th Symposium on Biological and Physiological Engineering, 299-302 (1989b) in Japanese.

Wood, J.E., Meek, S.G., Jacobsen, S.C.: Quantitation of human shoulder anatomy for prosthetic arm control - I Surface modelling. Journal of Biomechanics **22**, 3, 273-292 (1989a).

Wood, J.E., Meek, S.G., Jacobsen, S.C.: Quantitation of human shoulder anatomy for prosthetic arm control - II Anatomy matrices. Journal of Biomechanics **22**, 4, 309-325 (1989b).

Legend Descriptions

Figure 1:

Parallel-hierarchical neural network model. This learning control model can acquire the parallel inverse models structured by the inverse statics model ISM and the inverse dynamics model IDM, and arrange these parallel inverse models hierarchically in conjunction with a feedback controller FC. Controlling signals are the sum of the ISM output u_{ism}, the IDM output u_{idm} and the feedback signal u_{fc}.

Figure 2:

Redundancies at statics and dynamics levels. A Subscripts f and e denote flexor and extensor muscles. **B** The posture is specified as an intersection point of isometric length-tension curves for agonist and antagonist muscles. When the posture is maintained, there is an infinite number of combinations of the motor commands for a pair of muscles. **C** Muscle tensions for agonist and antagonist muscles during movement. There is also an infinite number of combinations of the muscle tensions for a pair of muscles, which is required to realize an intended trajectory.

Figure 3:

Human arm model with four single-joint muscles and two double-joint muscles.

Figure 4:

Stiffness ellipses predicted during posture maintenance in a horizontal plane. The shaded ellipse expresses the stiffness ellipse at the functional standard posture where the shoulder angle is 45 degrees and the elbow angle is 70 degrees.

Figure 5:

Target positions for point-to-point movements in a horizontal plane at the shoulder level.

Figure 6:

Stiffness ellipses predicted during movements in a horizontal plane. **A** 750-msec movements: (a) T2-T6; (b) T2-T5; (c) T3-T6; (d) T4-T1. **B** 500-msec movements: (a) T2-T6; (b) T2-T5; (c) T3-T6; (d) T4-T1.

Figure 7:

Virtual trajectories and tangential velocity profiles predicted during point-to-point movements in a horizontal plane. Solid line: desired. Dashed line: actual. Dotted line: virtual. **A** 750-msec movements: (a) T2-T6; (b) T2-T5; (c) T3-T6; (d) T4-T1. **B** 500-msec movements: (a) T2-T6; (b) T2-T5; (c) T3-T6; (d) T4-T1.

Figure 8:

Virtual trajectories predicted in joint coordinates. Solid, dashed and dotted lines show the desired, actual, and virtual trajectories, respectively. **A** 500-msec T2-T6 movement. **B** 500-msec T4-T1 movement.

Figure 9:

Motor commands to six muscles during T2-T6 750-msec movement. Solid curves: sum of the ISM and IDM outputs. Dotted curves: ISM output.

Figure 10:

Virtual trajectories predicted from the parameters that the at-rest shoulder stiffness is 6.44 N-m/rad and the at-rest elbow stiffness is 5.0 N-m/rad. Solid, dashed and dotted lines show desired, actual and virtual trajectories, respectively. **A** 750-msec T2-T6 movement. **B** 500-msec T2-T6 movement.

Figure 11:

Virtual trajectories predicted from the parameters that the at-rest shoulder stiffness is 21.6 N-m/rad and the at-rest elbow stiffness is 16.8 N-m/rad. Solid, dashed and dotted lines show desired, actual and virtual trajectories, respectively. **A** 750-msec T2-T6 movement. **B** 250-msec T2-T6 movement.

Figure 12:

ISM control using the straight desired trajectories based on the minimum-jerk model. Solid, dashed and dotted lines show the desired, actual, and virtual trajectories, respectively. **A** 750-msec movements: (a) T2-T6; (b) T2-T5; (c) T3-T6; (d) T4-T1. **B** 500-msec movements: (a) T2-T6; (b) T2-T5; (c) T3-T6; (d) T4-T1.

Figure 13:

A new computational scheme for learning control of arm movement which integrates the virtual trajectory control hypothesis and the feedback-error-learning scheme. VTP stands for the virtual trajectory planner, which calculates the necessary virtual trajectory while receiving the desired trajectory. Other notations are similar to those in Fig. 1. However, the feedback controller FC is designed in the Cartesian coordinates, and can be designed as the most simple PID feedback controller because the inverse kinematics problem needs not be addressed here. Correspondingly, because the input and the output of VTP are represented in the common Cartesian coordinates, it does not need to address the coordinate transformation problem from the Cartesian coordinates to the joint, muscle, or motor-command coordinates. However, VTP actually solves the inverse dynamics problem.

Table 1:

Arm parameters.

Table 2:

Moment arms: a_1 for shoulder flexor; a_2 for shoulder extensor; a_3 for elbow flexor; a_4 for elbow extensor; a_5 and a_6 for double-joint flexor; a_7 and a_8 for double-joint extensor.

Table 3:

Muscle parameters. The parameter r in Eq. (8c) is expressed as the joint angle in Eq. (10) corresponding to the rest length change with the motor command. The parameter l_m-l_0 in Eqs. (8c) and (10) is expressed as the angle corresponding to the difference between l_m and l_0.

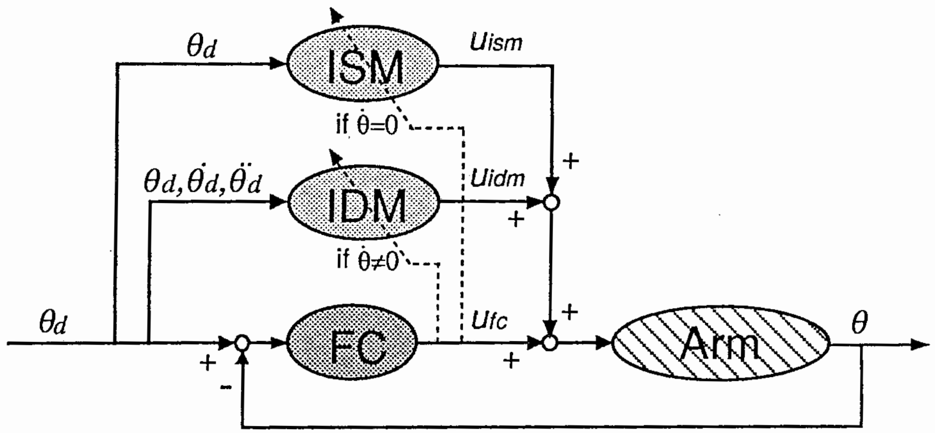

θ_d
ISM
u_{ism}
if $\dot{\theta}$=0
$\theta_d, \dot{\theta}_d, \ddot{\theta}_d$
IDM
u_{idm}
if $\dot{\theta}$≠0
θ_d
FC
u_{fc}
Arm
θ

Figure 1

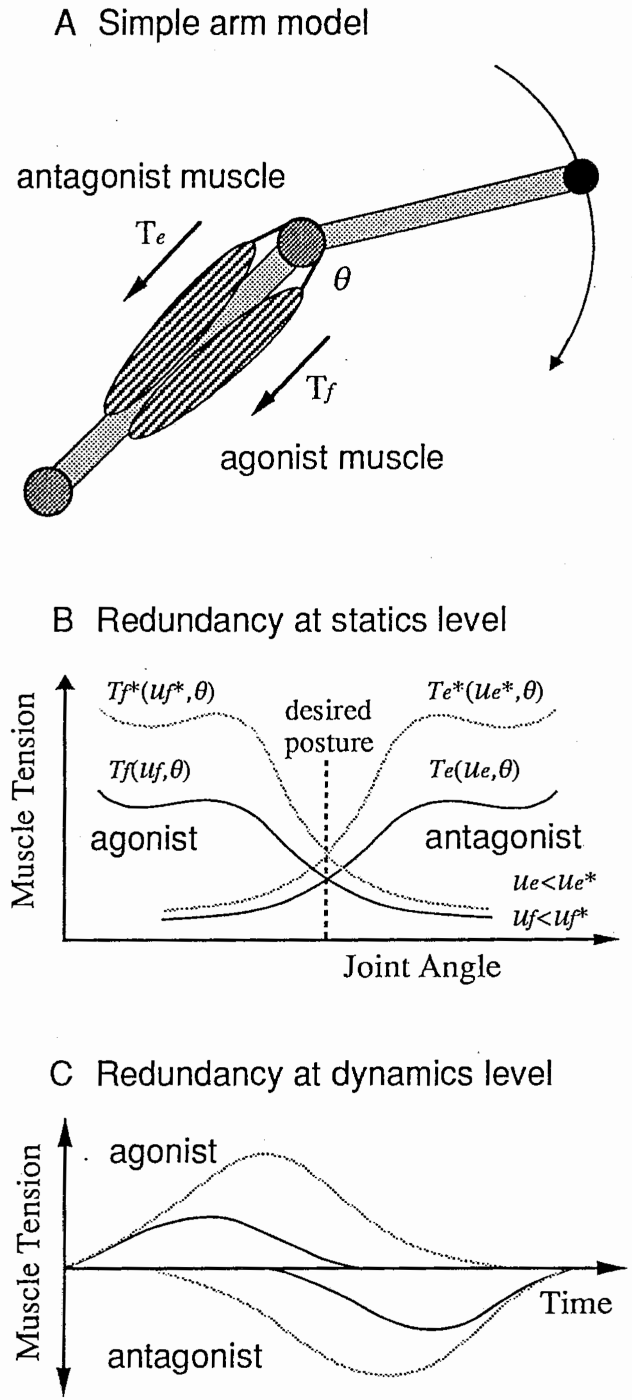
A Simple arm model
antagonist muscle
Te
θ
Tf
agonist muscle
B Redundancy at statics level
Muscle Tension
Tf*(uf*,θ)
desired posture
Te*(ue*,θ)
Tf(uf,θ)
Te(ue,θ)
agonist
antagonist
ue<ue*
uf<uf*
Joint Angle
C Redundancy at dynamics level
Muscle Tension
agonist
antagonist
Time

Figure 2

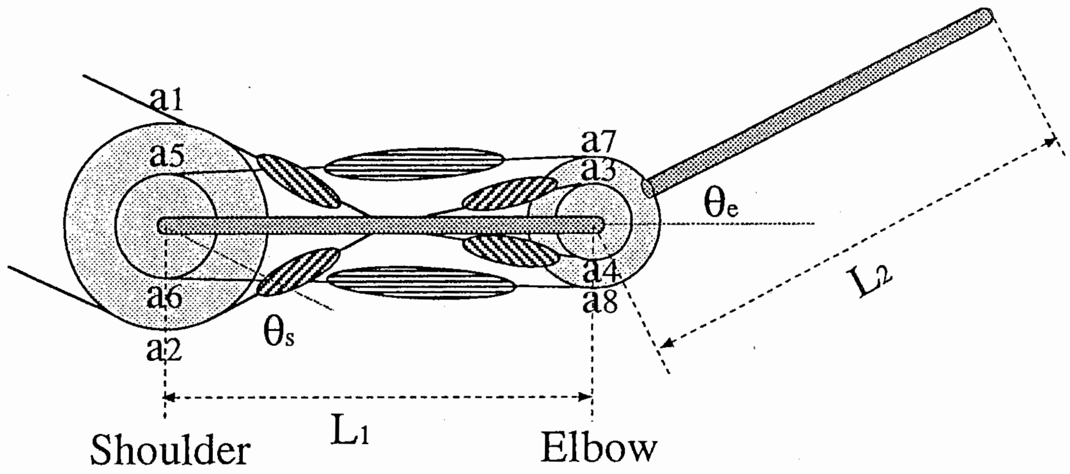

Figure 3

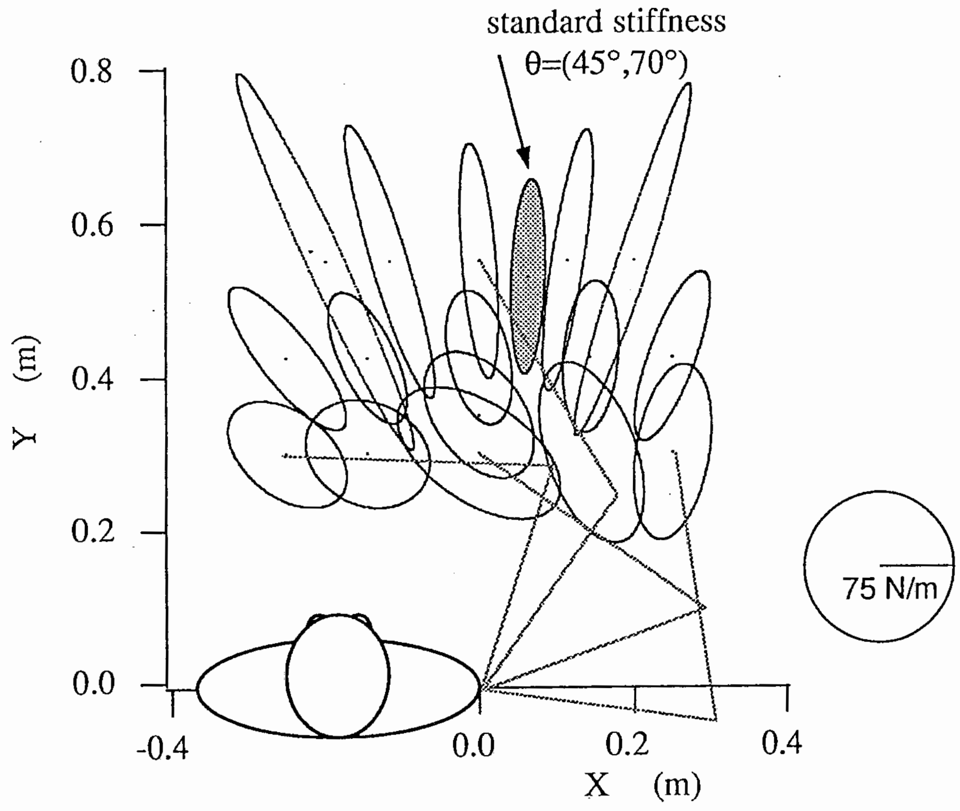

Figure 4

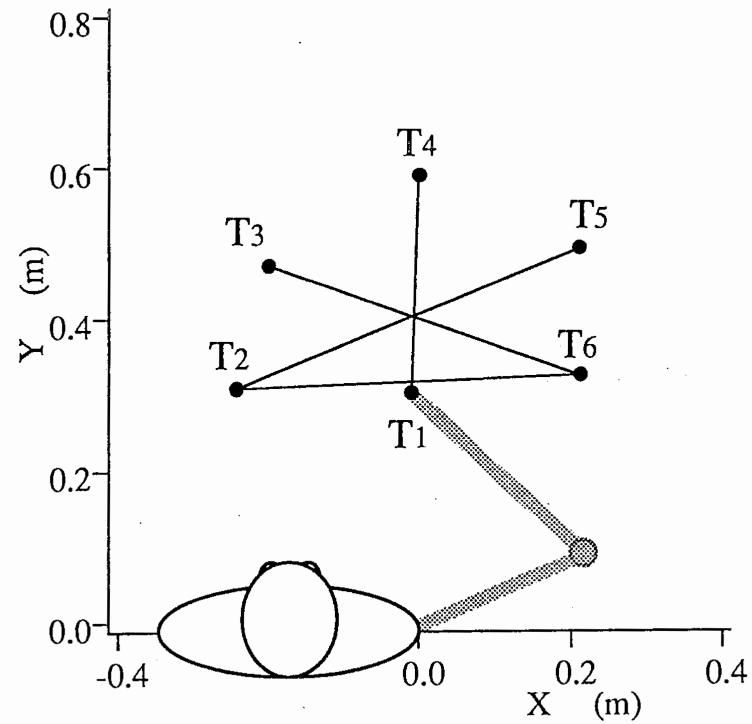

Figure 5

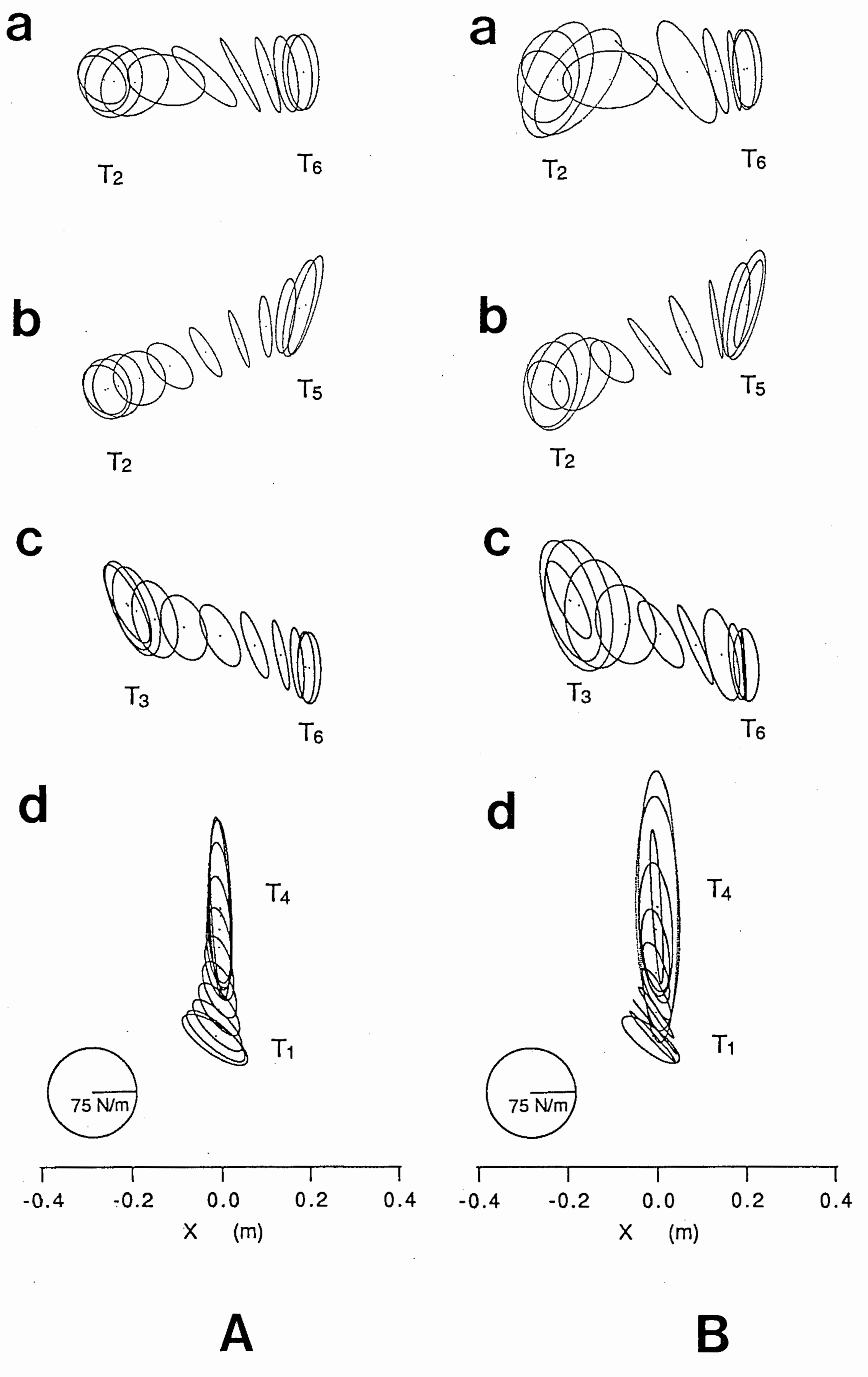
a
T2
T6
a
T2
T6
b
T2
T5
b
T2
T5
c
T3
T6
c
T3
T6
d
T4
T1
75 N/m
d
T4
T1
75 N/m
-0.4
-0.2
0.0
0.2
0.4
X (m)
-0.4
-0.2
0.0
0.2
0.4
X (m)
A
B

Fig. 6

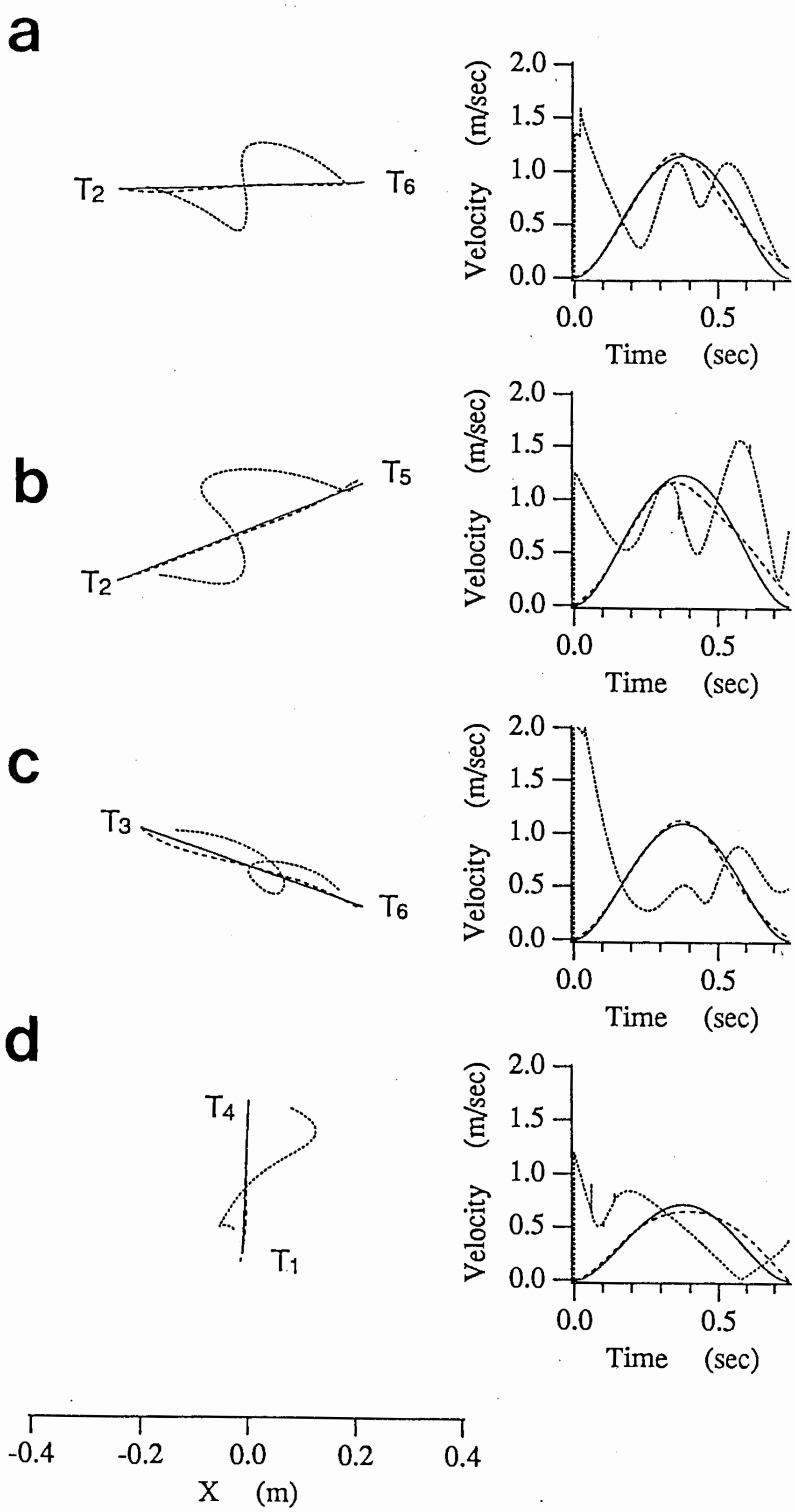
a
b
c
d
T2
T6
T2
T5
T3
T6
T4
T1
Velocity (m/sec)
Time (sec)
2.0
1.5
1.0
0.5
0.0
0.0
0.5
-0.4
-0.2
0.0
0.2
0.4
X (m)

Fig. 7 **A**

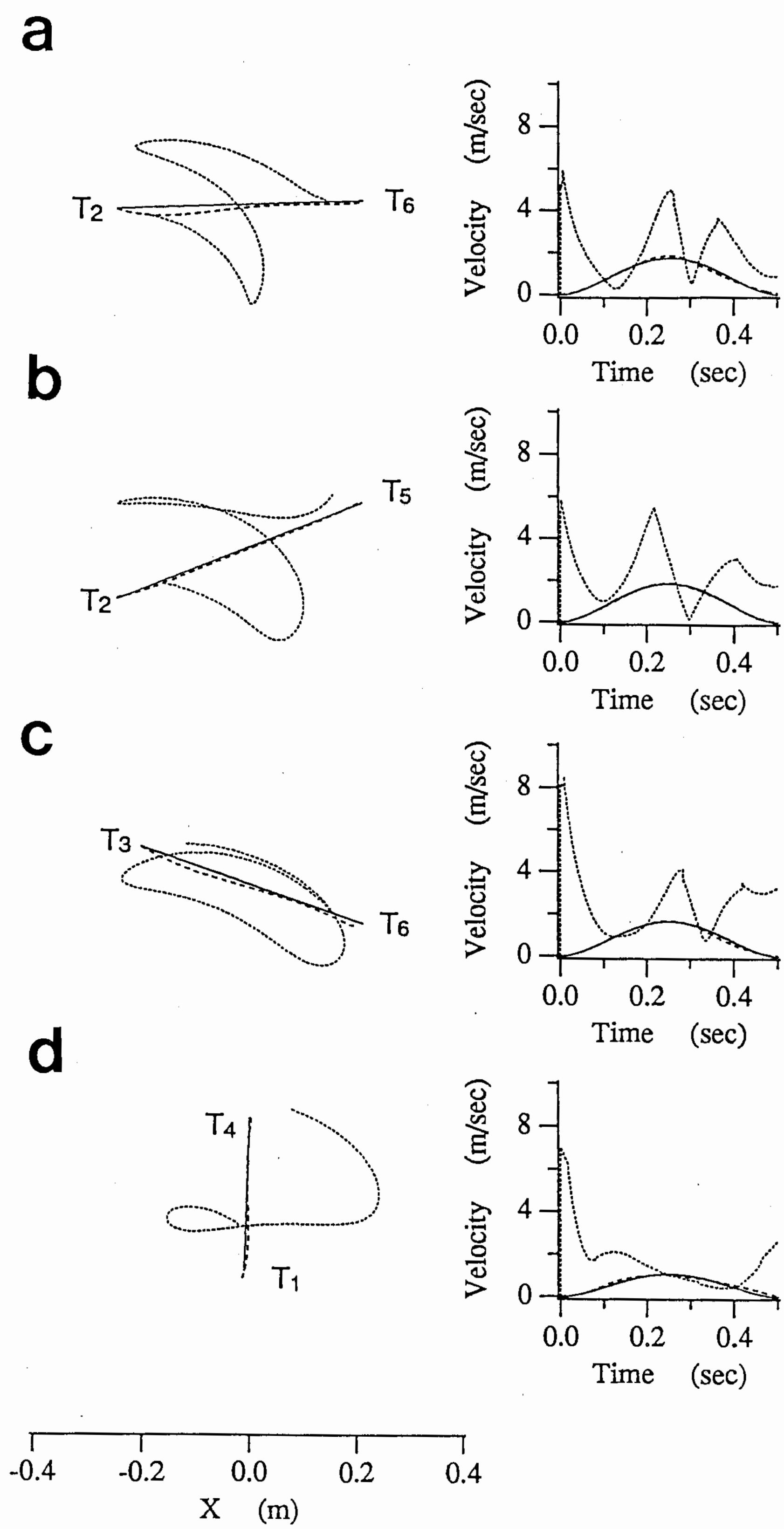

Fig. 7 **B**

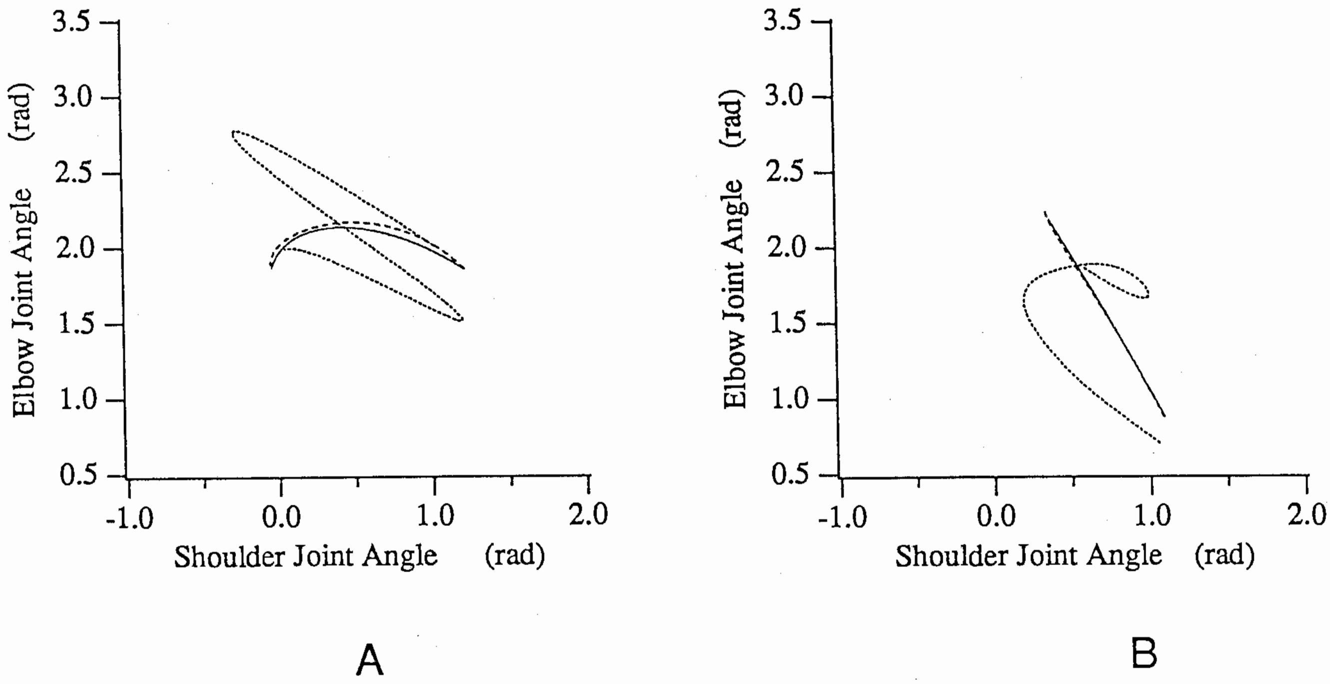
3.5
3.0
2.5
2.0
1.5
1.0
0.5
Elbow Joint Angle (rad)
-1.0
0.0
1.0
2.0
Shoulder Joint Angle (rad)
A
3.5
3.0
2.5
2.0
1.5
1.0
0.5
Elbow Joint Angle (rad)
-1.0
0.0
1.0
2.0
Shoulder Joint Angle (rad)
B

Fig. 8

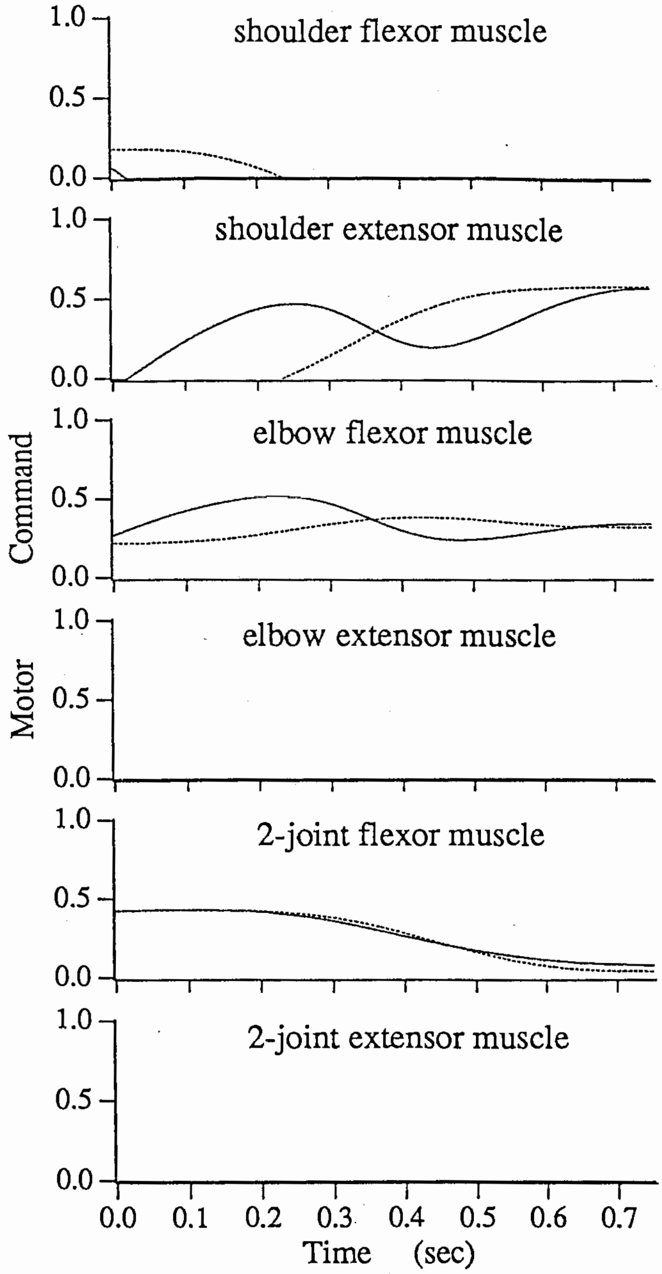
shoulder flexor muscle
shoulder extensor muscle
elbow flexor muscle
elbow extensor muscle
2-joint flexor muscle
2-joint extensor muscle
Motor Command
1.0
0.5
0.0
0.0 0.1 0.2 0.3 0.4 0.5 0.6 0.7
Time (sec)

Fig. 9

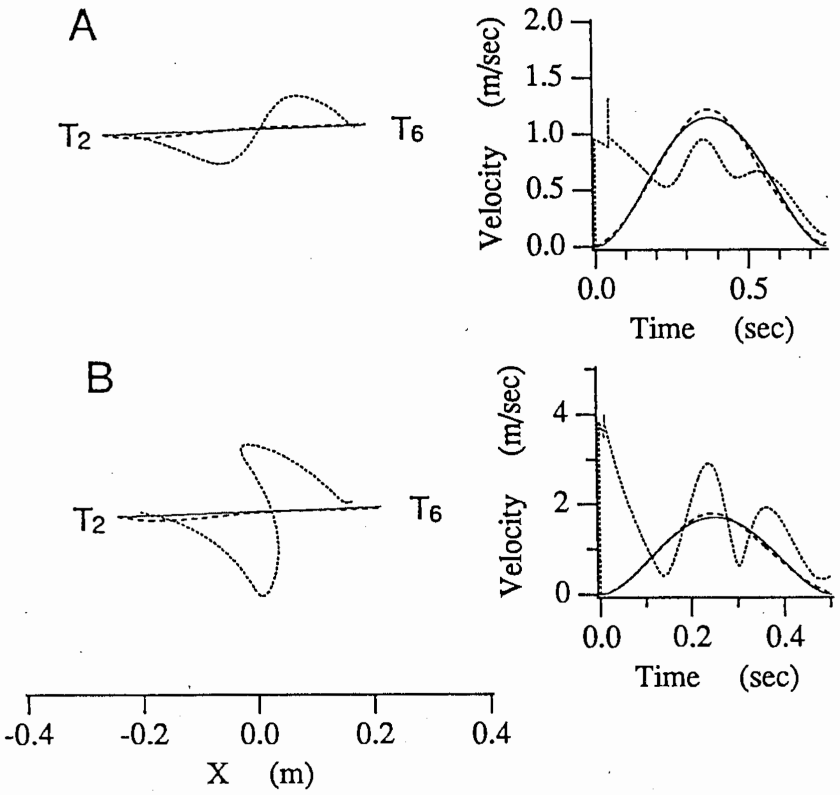
A
T2
T6
Velocity (m/sec)
2.0
1.5
1.0
0.5
0.0
0.0
0.5
Time (sec)
B
T2
T6
Velocity (m/sec)
4
2
0
0.0
0.2
0.4
Time (sec)
-0.4
-0.2
0.0
0.2
0.4
X (m)

Fig. 10

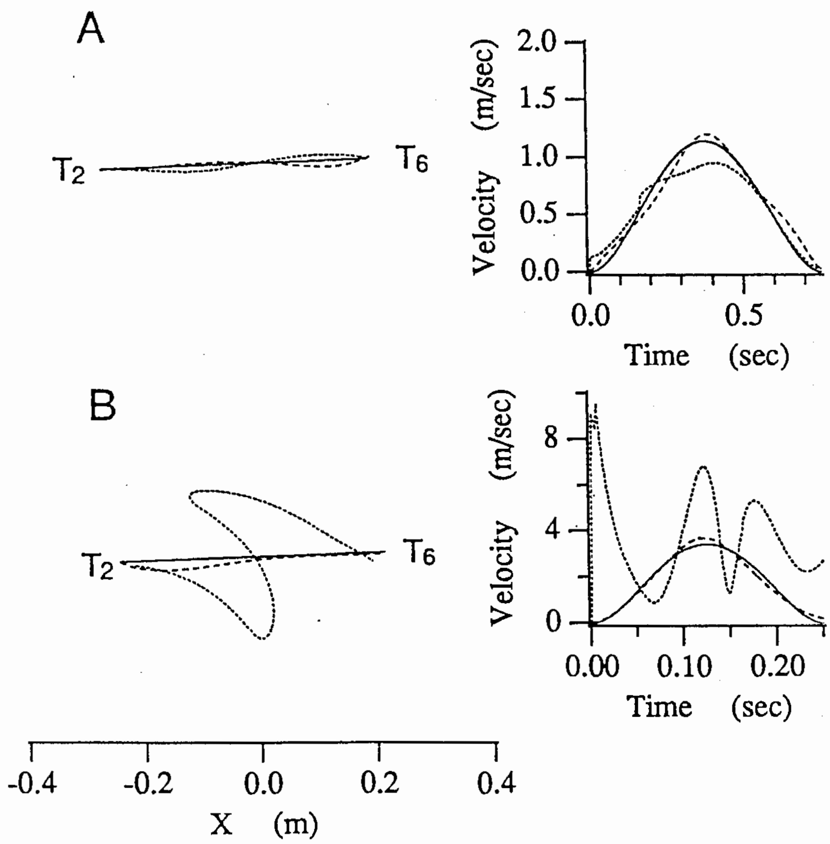
A
T2
T6
Velocity (m/sec)
2.0
1.5
1.0
0.5
0.0
0.0
0.5
Time (sec)
B
T2
T6
Velocity (m/sec)
8
4
0
0.00
0.10
0.20
Time (sec)
-0.4
-0.2
0.0
0.2
0.4
X (m)

Fig. 11

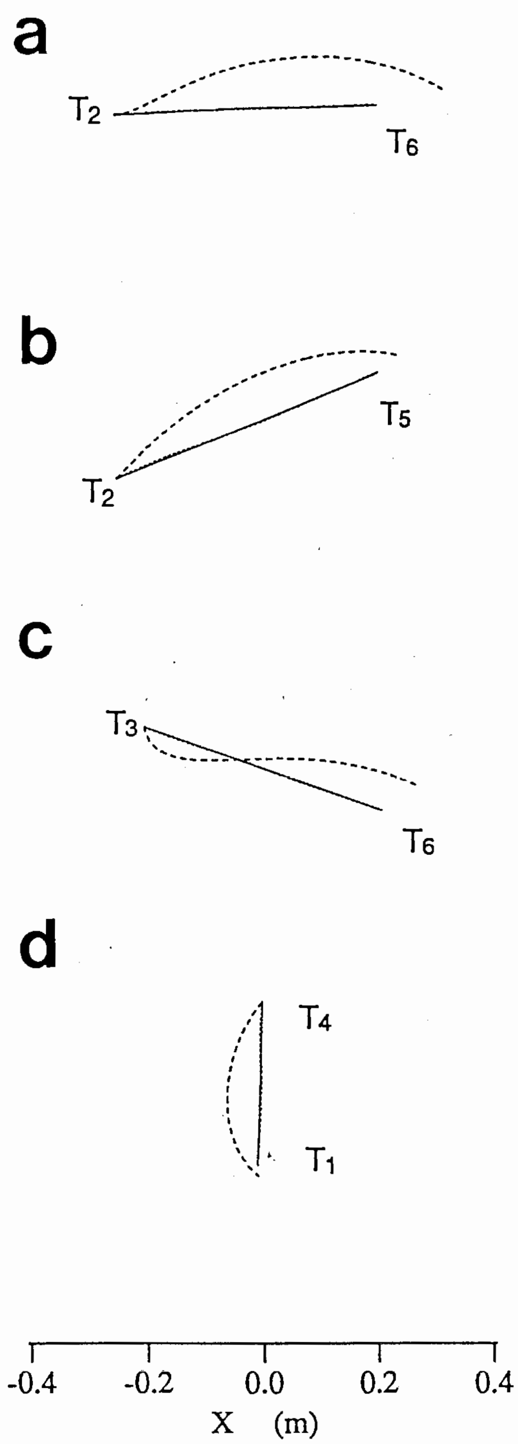

Fig. 12 **A**

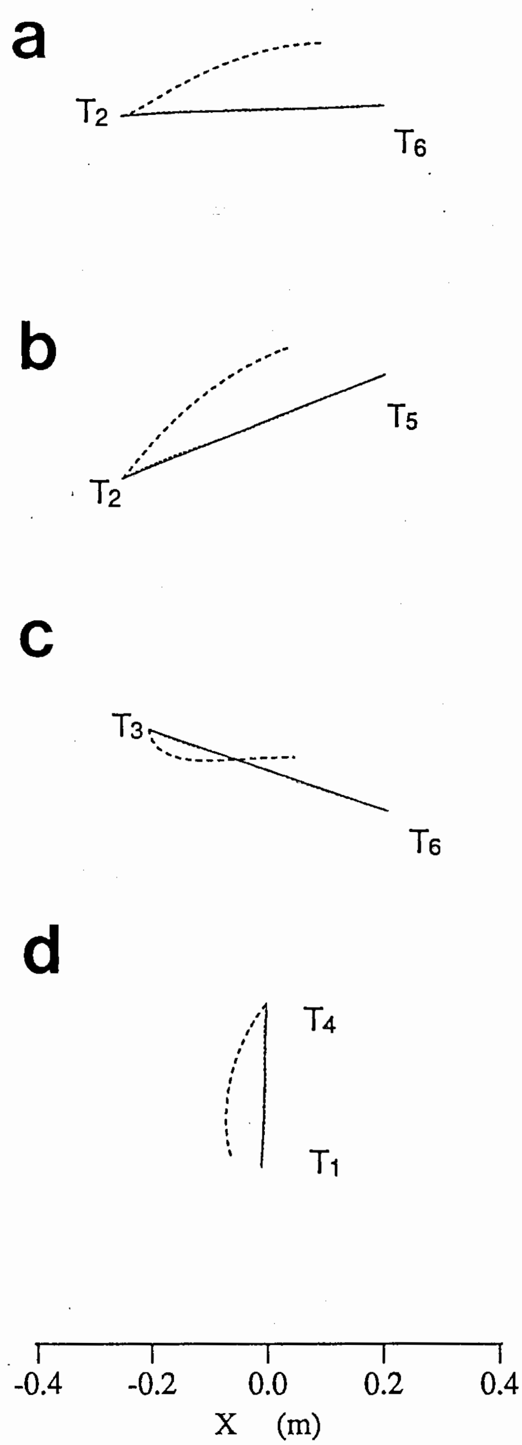

Fig. 12 **B**

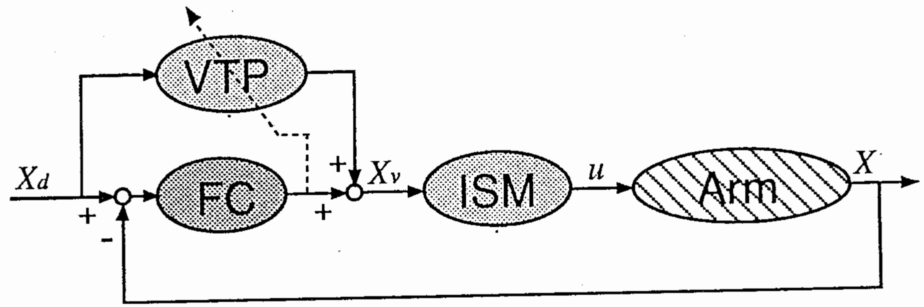

Fig 13

Table 1

	M (kg)	L (m)	Lg (m)	I (kgm^2)
$Link\,1$	1.59	0.3	0.18	0.0477
$Link\,2$	1.44	0.35	0.21	0.0588

Table 2

	a_1, a_2	a_3, a_4	a_5, a_6	a_7, a_8
$Moment\ Arm(cm)$	4.0	2.5	2.8	3.5

Table 3

	k (N/m)	k_0 (N/m)	b (Ns/m)	b_0 (Ns/m)	r $(Deg.)$	Angle corresponding to lm-lo $(Deg.)$
$Shoulder\ Flexor$	1621.6	810.8	108.1	54.1	-40°	180°
$Shoulder\ Extensor$	1621.6	810.8	108.1	54.1	40°	–90°
$Elbow\ Flexor$	1621.6	810.8	108.1	54.1	-40°	180°
$Elbow\ Extensor$	1621.6	810.8	108.1	54.1	40°	–40°
$2-Joint\ Flexor$	1621.6	810.8	108.1	54.1	-40°	360°
$2-Joint\ Extensor$	1621.6	810.8	108.1	54.1	40°	–130°